

Title page

Evaluation of the Relationship Between Cognitive Impairment, Glycometabolism, and Nicotinic Acetylcholine Receptor Deficits in a Mouse Model of Alzheimer's Disease

Yuki Matsuura¹, Masashi Ueda¹, Yusuke Higaki¹, Kohei Sano^{2,3}, Hideo Saji³, Shuichi Enomoto^{1,4}

¹Department of Biofunction Imaging Analysis, Graduate School of Medicine, Dentistry, and Pharmaceutical Sciences, Okayama University, 1-1-1 Tsushima naka, Kita-ku, Okayama 7008530, Japan

²Radioisotopes Research Laboratory, Kyoto University Hospital, 54 Kawaharacho, Shogoin, Sakyo-ku, Kyoto 6068507, Japan

³Department of Patho-Functional Bioanalysis, Graduate School of Pharmaceutical Sciences, Kyoto University, 46-29 Yoshida Shimoadachi-cho, Sakyo-ku, Kyoto 6068501, Japan

⁴Next-Generation Imaging Team, RIKEN Center for Life Science Technologies, 6-7-3 Minatojima-minatomachi, Chuo-ku, Kobe, Hyogo 6500047, Japan

Corresponding Author: Prof. Masashi Ueda

E-mail: mueda@cc.okayama-u.ac.jp

Running title: Relation of nAChR and cognition in AD

The manuscript category: Article

Abstract

Purpose

In patients with Alzheimer's disease (AD), the loss of cerebral nicotinic acetylcholine receptors (nAChRs) that are implicated in higher brain functions has been reported. However, it is unclear if nAChR deficits occur in association with cognitive impairments. The purpose of this study was to assess the relationship between nAChR deficits and cognitive impairments in a mouse model of AD (APP/PS2 mice).

Procedures

The cognitive abilities of APP/PS2 and wild-type mice (aged 2-16 months) were evaluated using the novel object recognition test. Double-tracer autoradiography analyses with 5-[¹²⁵I]iodo-A-85380 ([¹²⁵I]5IA: α 4 β 2 nAChR imaging probe) and 2-deoxy-2-[¹⁸F]fluoro-D-glucose were performed in both mice of different ages. [¹²³I]5IA-SPECT imaging was also performed in both mice at 12 months of age. Furthermore, each age cohort was investigated for changes in cognitive ability and expression levels of α 7 nAChRs and *N*-methyl-D-aspartate receptors (NMDARs).

Results

No significant difference was found between the APP/PS2 and wild-type mice at 2–6 months of age in terms of novel object recognition memory; subsequently, however, APP/PS2 mice showed a clear cognitive deficit at 12 months of age. [¹²⁵I]5IA accumulation decreased in the brains of 12-month-old APP/PS2 mice i.e., at the age at which cognitive impairments were first observed;

this result was supported by a reduction in the protein levels of $\alpha 4$ nAChRs using western blotting. nAChR deficits could be noninvasively detected by [123 I]5IA-SPECT *in vivo*. In contrast, no significant changes in glycometabolism, expression levels of $\alpha 7$ nAChRs, or NMDARs were associated with cognitive impairments in APP/PS2 mice.

Conclusion

A decrease in cerebral $\alpha 4\beta 2$ nAChR density could act as a biomarker reflecting cognitive impairments associated with AD pathology.

Key words

Alzheimer's disease, nicotinic acetylcholine receptors, 2-deoxy-2-[18 F]fluoro-D-glucose ([18 F]FDG), 5-[123 I]iodo-3-[2(*S*)-azetidylmethoxy]pyridine ([123 I]5IA), APP/PS2 mice

Introduction

Alzheimer's disease (AD), the most common chronic neurodegenerative disorder, is characterized by progressive cognitive impairments associated with a massive loss of synapses and neurons in the brain. At present, assessing its progression and severity requires several medical evaluations, such as mental state testing [1]. However, the results of these clinical diagnoses are frequently obscure because the current diagnosis of AD relies largely on the documentation of mental decline [2], and there is currently no definitive diagnostic test for assessing the cerebral functional changes that are fundamental to AD pathology. Thus, establishing a biomarker that reflects cognitive function is expected to aid in the understanding of the progression of AD and be beneficial clinically.

Nuclear medical imaging technology is a promising tool for *in vivo* monitoring of molecular processes using positron emission tomography (PET) and single-photon emission computed tomography (SPECT). Since this technique is non-invasive and highly quantitative, functional neuroimaging is being investigated as a possible method of identifying biomarkers for AD. Although much effort has been made to develop imaging probes for Amyloid- β ($A\beta$), one of the hallmark proteins in AD, $A\beta$ -PET imaging in patients with AD showed that the accumulation of $A\beta$ in the brain did not necessarily reflect the cognitive decline seen in these patients [3]. Furthermore, cerebral 2-deoxy-2- $[^{18}\text{F}]$ fluoro-D-glucose ($[^{18}\text{F}]$ FDG)-PET is used clinically as an index of central nervous system (CNS) activity. Although $[^{18}\text{F}]$ FDG-PET has been found to be better than other imaging modalities for AD diagnosis, it is difficult to use to characterize abnormal activity in late-onset

patients with AD [4].

Nicotinic acetylcholine receptors (nAChRs) in the CNS are reported to play an important role in higher brain functions, including learning, memory, and recognition [5]. Neuronal $\alpha 4\beta 2$ and $\alpha 7$ nAChRs are the two most predominant subtypes expressed in the CNS [6]. Thus, these subtypes are thought to be involved in the majority of nAChR signaling, and their dysfunction is believed to be related to several CNS disorders, including AD. Moreover, several acetylcholinesterase inhibitors, which target nAChRs directly or indirectly, have been developed for the treatment of AD and have been used successfully in the prevention of AD disease progression [7]. These inhibitors are reported to upregulate $\alpha 4\beta 2$ nAChRs and to protect neuronal cells against glutamate neurotoxicity, which has been implicated in AD [8]. Specifically, it has been reported that stimulation of $\alpha 4\beta 2$ nAChRs inhibits A β cytotoxicity [9]. Thus, $\alpha 4\beta 2$ nAChRs are one of the potential therapeutic targets to prevent the pathological progress of AD. Several imaging probes have been developed to visualize $\alpha 4\beta 2$ nAChRs using PET/SPECT, including 5- ^{123}I iodo-3-[2(*S*)-azetidylmethoxy]pyridine (^{123}I]5IA) [10] and 2- ^{18}F fluoro-3-[2(*S*)-azetidylmethoxy]pyridine (^{18}F]2FA), and some clinical studies in normal subjects and patients have been already successfully performed. Conversely, the characterization of $\alpha 7$ nAChR radioligands such as ^{18}F]ASEM and ^{18}F]NS10743 is still in progress, and no clinical research in patients has been conducted yet.

Several *in vivo* imaging studies using ^{18}F]2FA or ^{123}I]5IA in AD patients and age-matched healthy subjects have provided conflicting evidence regarding whether nAChR density is affected.

The majority of the available studies have shown significant reductions in tracer binding in AD [11-12]; however, there are some that have not [13]. A potential explanation for these heterogeneous results is that clinical trials are directly affected by factors such as secondhand smoke and the varying combination of symptoms. As a complement to clinical studies, many types of transgenic mice have recently been developed with expressions of specific altered genes that relate to human diseases. Thus, studies using transgenic mice as animal models of AD would be more useful than clinical trials to elucidate directly whether the nAChR deficits occur in association with cognitive impairments or not.

In this study, we aimed to investigate the age-related changes in cognitive function, cerebral glucose metabolism, and nAChR expression in the brain as the disease advances using an AD mouse model (APP/PS2 mouse). Our [¹²⁵I]5IA-autoradiography (ARG) analysis showed that $\alpha 4\beta 2$ nAChR deficits in the brains of APP/PS2 mice occurred when cognitive impairment was first observed. It was supported by a reduction in $\alpha 4$ nAChRs protein levels, as detected by western blotting. The [¹²³I]5IA-SPECT analysis was sufficiently sensitive to assess the decline in $\alpha 4\beta 2$ nAChRs in the brains of APP/PS2 mice at 12 months of age. Conversely, changes in glucose uptake and $\alpha 7$ nAChR expression were not associated with cognitive impairments in the AD model. This suggests that decreased $\alpha 4\beta 2$ nAChRs density in the brain acts as an imaging biomarker that reflects the state of cognitive function in AD.

Materials and methods

Animals

Animal experiments were performed in accordance with the guidelines of the Okayama University and Kyoto University Animal Care Committees. The experimental procedures performed were approved by both care committees. All studies were conducted with Tg2576×PS2 (APP/PS2) double-transgenic mice [14] and age-matched wild-type littermate controls. Male Tg2576 and female PS2 mice were purchased from Taconic Biosciences, Inc. (Hudson, NY, USA) and Oriental Yeast Co., Ltd. (Tokyo, Japan), respectively. To obtain APP/PS2 mice, Tg2576 mice were crossed with PS2 mice.

Materials

Sodium [^{125}I]iodide and sodium [^{123}I]iodide were purchased from PerkinElmer (MA, USA) and FUJIFILM RI Pharma Co., Ltd. (Tokyo, Japan), respectively, and radioiodination of [$^{123/125}\text{I}$]5IA was performed according to our previous report [15]. [^3H]MK-801 were purchased from American Radiolabeled Chemicals Inc. (MO, USA). [^{18}F]FDG was provided by Kyoto University Hospital (Kyoto, Japan).

Novel object recognition test

The novel object recognition (NOR) test was performed on all APP/PS2 and wild-type mice

used at 2, 6, 12, and 16 months of age (n = 9–21 per group) using a modification of the procedure by Oulès *et al.*[16]. This test was conducted in an open field (44 × 44 cm). Initially, the animals were habituated to the environment for 10 min/day for 3 days. On day 4, two identical objects (50-mL conical polypropylene tubes) were placed in the field, and animals were allowed to explore the objects for 10 min. On day 5, the animals were returned to the area with one familiar object (50-mL conical polypropylene tube) and one novel object (brown glass bottle) and allowed to explore the objects for 5 min. The time spent exploring each object was recorded and analyzed using ANY-maze software (Stoelting Co., IL, USA). An exploration preference (EP) index was calculated as follows: EP values (%) = time spent exploring the novel object / (time spent exploring the novel object + time spent exploring the familiar object) × 100. Animals that spent < 8 s exploring the objects during the 10-min training session were omitted from the analysis (1–9 mice per group).

Ex vivo dual autoradiography with [¹²⁵I]5IA and [¹⁸F]FDG

APP/PS2 and wild-type mice at 2, 6, 12, and 16 months of age (n = 4–5 per group) were deprived of food for 12–15 h after which the mice received injections of a mixture of [¹²⁵I]5IA (700 kBq) and [¹⁸F]FDG (23 MBq) via the tail vein. All mice were killed by decapitation 60 min after the injection. The brains were rapidly removed and frozen followed by slicing into 10 µm thick sections using a microtome. Two serial sections per brain region were exposed to an imaging plate (BAS IP SR; Fuji Photo Film, Tokyo, Japan) for 1 h together with the calibrated ¹⁸F standards ([¹⁸F]FDG

solution) to obtain [¹⁸F]FDG autoradiograms. After complete attenuation of the radioactivity of ¹⁸F, the radioactivity resulting from [¹²⁵I]5IA was determined by exposure to a new imaging plate for 12 h together with the calibrated ¹²⁵I standards ([¹²⁵I]5IA solution). Autoradiographic images were gained and analyzed as reported previously [10]. Two independent measurements were taken from the thalamus, cerebellum, striatum, cerebral cortex, hippocampus identified using a mouse brain atlas. The accumulation of radioactivity within regions of interest (ROIs) was calculated according to the following equation corrected for injection dose (MBq) and body weight (g): radioactivity accumulation (%ID*BW) = (radioactivity for each ROI) / (injected radioactivity / animal body weight) × 100.

Histological staining of Amyloid β

Upon completion of the *ex vivo* dual autoradiography study, serial sections were stained with thioflavin-S using the same procedure as that stated by Iikuni *et al.*[17]. The digital images (n = 4 per group) taken under the same conditions were analyzed with BZ-X analyzer ver. 1.3.1.1 software (Keyence Corp., Osaka, Japan). The area of interest of the hippocampus and cortex were manually outlined in each image, and the areas stained by thioflavin-S were quantified.

SPECT/CT imaging

After injection of [¹²³I]5IA (4.6–7.6 MBq) into each APP/PS2 and wild-type mouse (n = 4–5) via the tail vein, dynamic SPECT/CT imaging was conducted using the same methods as those in our previous report [15]. For an accurate ROI definition, each mouse was subjected to magnetic resonance (MR) brain imaging one day prior to SPECT/CT imaging. Two spheroidal ROIs in the frontal cortex, striatum, hippocampus, thalamus, and cerebellum were positioned on MR images and then applied to SPECT images, as previously reported [15]. Standardized uptake values (SUVs) were calculated according to the following equation: SUV = radioactivity for each ROI (kBq/cc) / (injected dose [kBq] / body weight [g]) × 100.

Immunoblotting

The hippocampus of APP/PS2 and wild-type mice at 2, 12, and 16 months of age (n = 4 per group) were homogenized in a radioimmunoprecipitation assay buffer containing protease inhibitor. The electrophoresis and immunoblotting were performed via the same procedure as that stated by Oulès *et al.*[16]. The antibody resources and the details for application are shown in Supplemental Table 1.

Statistical analysis

GraphPad Prism ver. 7 (GraphPad, San Diego, CA, USA) was used for all statistical analyses. The comparisons between two groups were performed with student's *t*-test. The statistical

data among 3 or more groups were assessed by analysis of variance (ANOVA) with a Bonferroni's post-hoc test. Correlation coefficients were assessed using Pearson's analysis. Differences with a P value < 0.05 were considered to be statistically significant. All data are expressed as mean \pm standard deviation (SD).

Results

Amyloid load of APP/PS2 mice

Figure 1 shows the time-dependent changes in A β deposition in the brains of APP/PS2 mice. The presence of A β plaques was first observed at 6 months of age. After 12 months of age, the amyloid- β plaque loads in the hippocampus and cortex were significantly increased compared to 2 and 6 months of age ($*P < 0.05$, $**P < 0.01$, $***P < 0.001$, $****P < 0.0001$ between indicated groups, $n = 4$ mice per group). Conversely, no plaque was found in the wild-type mice at any age (data not shown).

Novel object recognition test

Figure 2 shows the time-dependent changes in cognitive abilities (expressed as EP values) of APP/PS2 and wild-type mice. No significant difference was found between the APP/PS2 and wild-type mice at 2–6 months of age in terms of novel object recognition memory. However,

APP/PS2 mice at 12 months of age showed a clear reduction in EP values as compared with those of wild-type mice ($P < 0.0001$), and APP/PS2 mice at 16 months of age showed the same level of cognitive deficit as at 12 months of age ($P < 0.01$). Conversely, no significant differences were found in EP values in wild-type mice at any age.

Autoradiographic analysis of cerebral glucose metabolism

Figure 3 shows the age-related changes in [^{18}F]FDG uptake in each brain region of the APP/PS2 and wild-type mice. No significant differences were observed in any of the brain regions of the APP/PS2 mice at 2 months of age as compared with in wild-type mice. At 6 months of age, glucose uptake tended to increase in the cortex and hippocampus of APP/PS2 mice as compared with in wild-type mice. This tendency was terminated in all brain regions in APP/PS2 mice at 12 months of age, however, and at 16 months of age, glucose metabolism tended to decrease in the hippocampus and thalamus of APP/PS2 mice as compared with in the wild-type mice. However, these differences mentioned above were not statistically significant in any group. No age-related change in glucose metabolism was detected in the wild-type mice.

Autoradiographic analysis of nAChR density

Figure 4 shows age-related changes in [^{125}I]5IA accumulation in all brain regions in the APP/PS2 and wild-type mice. The accumulation pattern of [^{125}I]5IA in the brain of wild-type mice

was consistent with the known distribution pattern of $\alpha 4\beta 2$ nAChRs with the highest accumulation in the thalamus; moderate in the striatum, hippocampus, and cerebral cortex; and the lowest in the cerebellum. No age-related change in [^{125}I]5IA accumulation was detected in the wild-type mice.

As compared with wild-type mice, no significant difference was observed in any of the brain regions examined at 2 months of age in APP/PS2 mice. At 6 months, [^{125}I]5IA accumulation tended to increase in the hippocampus of APP/PS2 mice as compared with in wild-type mice, and showed almost the same levels in the other four brain regions as that noted in the wild-type mice. In 12-month-old APP/PS2 mice, however, the [^{125}I]5IA accumulation decreased in the cortex, hippocampus, and thalamus ($P < 0.05$, $n = 4-5$ per group) in comparison with the results seen in the wild-type mice. Decreases in [^{125}I]5IA accumulation were maintained in all brain regions of the APP/PS2 mice at 16 months of age (striatum: $P < 0.05$, cortex: $P < 0.01$, hippocampus and thalamus: $P < 0.0005$, $n = 4-5$ per group). In contrast, no significant difference was found in [^{125}I]5IA accumulation in the cerebellum in both groups at all the ages examined.

SPECT imaging with [^{123}I]5IA

Figure 5a shows SPECT/CT images of the APP/PS2 and wild-type mice obtained 56 min after injection of [^{123}I]5IA. Images show slices at the frontal cortical, thalamic, and cerebellar levels, respectively. The accumulation pattern of [^{123}I]5IA in the brains of wild-type mice was consistent with the known distribution pattern of $\alpha 4\beta 2$ nAChRs. The averaged SUVs in each brain region of

both mice are shown in Figure 5b. The SPECT signals in the frontal cortex and hippocampus ($P < 0.01$), and thalamus ($P < 0.05$) of APP/PS2 mice were lower than those detected in wild-type mice ($n = 4-5$ per group). In contrast, no significant difference was found in SUVs in the cerebellum. These findings were consistent with the results obtained in the ARG study. However, it should be noted that due to the low spatial resolution of SPECT images, radioactivity in the hippocampus, as determined by SPECT imaging, may be overestimated by the influence of high radioactivity in the thalamus.

Expression levels of nAChRs

To confirm that reduced [125 I]5IA accumulation was detected in the brains of APP/PS2 mice at 12 and 16 months of age, we measured the protein levels of $\alpha 4$ and $\beta 2$ nAChRs. As shown in Figure 6, the $\alpha 4$ subunit was reduced at the protein level by 30% ($P < 0.01$) in the hippocampus of APP/PS2 mice at 16 months of age as compared with in the wild-type mice at the same age. There were no significant differences in the protein levels of $\beta 2$ nAChRs between the APP/PS2 and wild-type mice at any age. Additionally, reverse transcription polymerase chain reaction (RT-PCR) analyses revealed no significant change in the mRNA levels of $\alpha 4$ and $\beta 2$ nAChRs in APP/PS2 mice at 2, 6, 12, or 16 months of age, as compared with wild-type mice of the same ages (Supplemental Figure 1).

We also measured the protein levels (Figure 6) and the mRNA expression levels (Supplemental Figure 1) of $\alpha 7$ nAChR. APP/PS2 mice showed elevated $\alpha 7$ nAChR protein levels in

the hippocampus at 12 and 16 months of age (Figure 6, $P < 0.01$), and also showed elevated $\alpha 7$ nAChR mRNA levels in the hippocampus at 2-16 months of age (2 months: $P < 0.05$, 6 months: $P < 0.01$, 12 and 16 months: $P < 0.0001$, Supplemental Figure 1) in comparison with the wild-type mice.

Autoradiographic analysis of NMDAR density

The age-related changes in [^3H]MK-801 binding in each brain region of the APP/PS2 and wild-type mice were evaluated and the results were shown in Supplemental Figure 2. No significant difference was observed in any brain region at any month of age in both mice.

Discussion

In this study, we explored the relationship between nAChR deficits, glycometabolism, and cognitive impairments in the presence of amyloid in an APP/PS2 AD mouse model. Double-tracer autoradiography (ARG) analysis and SPECT imaging study showed that [$^{123/125}\text{I}$]5IA accumulation decreased in the cortex, hippocampus, and thalamus of 12-month-old APP/PS2 mice as compared with that recorded in the wild-type controls, i.e., at the age when cognitive impairments were first observed. Reductions in the protein levels of $\alpha 4$ nAChRs were also detected in the brains of 16-month-old APP/PS2 mice using Western blotting. However, changes in glucose uptake and $\alpha 7$ nAChR expression were not associated with cognitive impairment.

In the present study, we focused on nAChRs as targets for imaging biomarkers that might be used to identify the cognitive impairments induced by amyloid pathology, because nAChRs are reported to play an important role in cognitive function [5]. In addition, NMDARs are also reported to be involved in the cognitive impairments seen in AD, and are one of the targets for AD treatment [18]. Therefore, we evaluated the density of NMDARs in APP/PS2 mice using an *in vitro* ARG analysis of [³H]MK-801. However, no significant difference in [³H]MK-801 binding was observed between the APP/PS2 and wild-type mice (Supplemental Figure 2). These results suggest that rather than the density of NMDAR, the density of $\alpha 4\beta 2$ nAChR might be a more sensitive biomarker for the cognitive impairments induced by amyloid pathology.

The NOR test is a validated method for evaluating object cognition and recognition memory [16]. In the present study, APP/PS2 mice exhibited clear cognitive deficits at 12 and 16 months of age, when compared with wild-type mice. Using the Morris water maze test, Toda *et al.* reported that APP/PS2 mice exhibited impaired spatial learning and memory abilities at 4-5 months of age [14]. Impairment of spatial learning seems to occur earlier than that of object recognition. This discrepancy is consistent with a previous report that cognitive impairment occurs in APP/PS1 and Tg2576 mice 1-13 months later when assessed by the NOR task rather than by the Morris water maze task [19]. Not all tasks have yielded similar findings, which may be a result of each task assessing different cognitive domains or behavioral aspects. It is possible that brain regions showing a decreased expression of $\alpha 4\beta 2$ nAChRs in the present study are involved in object cognition and

recognition memory, not spatial learning.

Our [^{18}F]FDG-ARG analysis showed that glucose uptake increased in the cortex and hippocampus of APP/PS2 mice at 6 months of age as compared with wild-type mice. A previous [^{18}F]FDG-PET study also reported significant cerebral hypermetabolism in APP/PS1 mice at six months of age [20]. Conversely, the increased glucose uptake that has been shown in several AD mouse models is clearly different from the decreased glucose uptake observed in human patients with AD. The reason for the discrepancy is unclear, but it is hypothesized that increased Ca^{2+} signaling and inflammatory responses by microglia and astrocytes affect glucose uptake [21]. Nine-month-old PS2APP mice are reported to show the first signs of an inflammatory response, as revealed by CD45 immunoreactivity and [^3H]PK11195 binding analyses [22]. Thus, [^{18}F]FDG might detect the neuropathological inflammatory response in the CNS. An electron microscopy study previously revealed the presence of extracellular $\text{A}\beta$ and found that increased levels of insoluble $\text{A}\beta$ were present in five-month-old APP/PS2 mice [14]. Characterization of the age-related changes in intraneuronal/extraneuronal oligomer deposition would provide further information on the relationship between glycometabolism and amyloid pathology in APP/PS2 mice.

Since nAChRs are reported to be involved in higher brain function such as memory and recognition abilities, decreased $\alpha 4\beta 2$ nAChR density could be used as a sensitive biomarker for cognitive impairments related to amyloid pathology. In this study, $\alpha 4\beta 2$ nAChR deficits in the brains of APP/PS2 mice occurred at 12 months of age, which is when the cognitive impairment was first

observed. We found deficits in $\alpha 4\beta 2$ nAChR at the protein level, but not at the genetic mRNA level. The discrepancy may be caused by alteration of nAChR synthesis on a different level, such as translation or post-translation modifications, or receptor turnover [23]. Conversely, the mRNA and protein levels of $\alpha 7$ nAChR subunits were significantly higher in the brains of APP/PS2 mice than in wild type mice. Interestingly, a reduction in $\alpha 7$ nAChR levels has been reported in the brains of patients with AD, while an increase in $\alpha 7$ nAChRs was recently detected in PC-12 cells exposed to 5 μM $\text{A}\beta_{1-42}$ [24]. Since at 6-7 months of age, PS2APP mice showed higher levels of insoluble $\text{A}\beta_{1-42}$ in their brains than those observed in AD patients [14], it could be hypothesized that enhanced expression of $\alpha 7$ nAChR subunits was stimulated directly by higher concentrations of $\text{A}\beta_{1-42}$. Moreover, $\alpha 7$ nAChRs are reported to be essential for inhibiting cytokine synthesis via the cholinergic anti-inflammatory pathway [25]. In the brain of patients with AD, $\alpha 7$ nAChRs may serve an anti-inflammatory role affecting neuropathological inflammation. This may be one of the reasons why $\alpha 7$ nAChRs were upregulated in the brain of APP/PS2 mice. The discrepancy between the decline in $\alpha 4\beta 2$ nAChR subunits and increased density of $\alpha 7$ nAChR subunits would be an interesting focal point for AD pathology, and a potential topic for further studies.

Our previous research provided the first evaluation of SPECT imaging of $\alpha 4\beta 2$ nAChRs in the mouse brain [15]. In this study, the [^{123}I]5IA-SPECT analysis was sufficiently sensitive to detect the decline in $\alpha 4\beta 2$ nAChRs in the brains of APP/PS2 mice at 12 months of age. Therefore, measuring $\alpha 4\beta 2$ nAChR density using [^{123}I]5IA-SPECT may help in the evaluation of cognitive

abilities in AD mouse models, and in the screening of drugs targeting nAChRs.

Conclusions

The deficits of $\alpha 4\beta 2$ nAChR in the brain of an AD mouse model (involving APP/PS2 mice) occurred at 12 months of age, which is when cognitive impairment was first observed. NACHR deficits could be noninvasively detected by [123 I]5IA-SPECT *in vivo*. In contrast, no significant changes in glycometabolism, expression levels of $\alpha 7$ nAChRs, or NMDARs were associated with cognitive impairments in APP/PS2 mice. This result suggests that a reduction in $\alpha 4\beta 2$ nAChR density in the brain might act as an imaging biomarker that reflects cognitive function in AD.

Acknowledgments

This work was supported in part by a Grant-in-Aid for COE projects by MEXT, Japan, titled "Center of excellence for molecular and gene targeting therapies with micro-dose molecular imaging modalities", a Grant-in-Aid for Challenging Exploratory Research (KAKENHI No. 26670562 and 16K15583) from the Japan Society for the Promotion of Science, and a grant from the Smoking Research Foundation. Yuki Matsuura gratefully acknowledged the funding received from Nagai Memorial Research Scholarship from the Pharmaceutical Society of Japan.

Conflict of Interest

The authors declare that they have no conflicts of interest.

References

1. McKhann GM, Knopman DS, Chertkow H, et al. (2011) The diagnosis of dementia due to Alzheimer's disease: Recommendations from the National Institute on Aging-Alzheimer's Association workgroups on diagnostic guidelines for Alzheimer's disease. *Alzheimers Dement.* 7:263-269.
2. Milne A, Culverwell A, Guss R, Tuppen J, Whelton R (2008) Screening for dementia in primary care: a review of the use, efficacy and quality of measures. *Int Psychogeriatr.* 20:911-926.
3. McConathy J, Sheline YI (2015) Imaging biomarkers associated with cognitive decline: a review. *Biol Psychiatry.* 77:685-692.
4. Yasuno F, Imamura T, Hirono N, et al. (1998) Age at onset and regional cerebral glucose metabolism in Alzheimer's disease. *Dement Geriatr Cogn Disord.* 9:63-67.
5. Levin ED, Simon BB (1998) Nicotinic acetylcholine involvement in cognitive function in animals. *Psychopharmacology.* 138:217-230.
6. Alkondon M, Albuquerque EX (2001) Nicotinic acetylcholine receptor alpha 7 and alpha 4 beta 2 subtypes differentially control GABAergic input to CA1 neurons in rat hippocampus. *J Neurophysiol.* 86:3043-3055.
7. Maelicke A, Samochocki M, Jostock R, et al. (2001) Allosteric sensitization of nicotinic receptors by galantamine, a new treatment strategy for Alzheimer's disease. *Biol Psychiatry* 49:279-288.

8. Akaike A, Takada-Takatori Y, Kume T, Izumi Y (2010) Mechanisms of Neuroprotective Effects of Nicotine and Acetylcholinesterase Inhibitors: Role of alpha 4 and alpha 7 Receptors in Neuroprotection. *J Mol Neurosci* 40:211-216.
9. Kihara T, Shimohama S, Urushitani M, et al. (1998) Stimulation of alpha 4 beta 2 nicotinic acetylcholine receptors inhibits beta-amyloid toxicity. *Brain Res* 792:331-334.
10. Saji H, Ogawa M, Ueda M, et al. (2002) Evaluation of radioiodinated 5-iodo-3-(2(S)-azetidylmethoxy)pyridine as a ligand for SPECT investigations of brain nicotinic acetylcholine receptors. *Ann Nucl Med* 16:189-200.
11. O'Brien JT, Colloby SJ, Pakrasi S, et al. (2007) alpha 4 beta 2 nicotinic receptor status in Alzheimer's disease using ¹²³I-5IA-85380 single-photon-emission computed tomography. *J Neurol Neurosurg Psychiatry*. 78:356-361.
12. Terriere E, Sharman M, Donaghey C, et al. (2008) alpha 4 beta 2-nicotinic receptor binding with 5-IA in Alzheimer's disease: Methods of scan analysis. *Neurochem Res*. 33:643-651.
13. Mitsis EM, Reech KM, Bois F, et al. (2009) ¹²³I-5IA-85380 SPECT Imaging of Nicotinic Receptors in Alzheimer Disease and Mild Cognitive Impairment. *J Nucl Med* 50:1455-1463.
14. Toda T, Noda Y, Ito G, Maeda M, Shimizu T (2011) Presenilin-2 Mutation Causes Early Amyloid Accumulation and Memory Impairment in a Transgenic Mouse Model of Alzheimer's Disease. *J Biomed Biotechnol*. 2011:617974.
15. Matsuura Y, Ueda M, Higaki Y, et al. (2016) Noninvasive evaluation of nicotinic

acetylcholine receptor availability in mouse brain using single-photon emission computed tomography with ¹²³I-5IA. Nucl Med Biol. 43:372-378.

16. Oules B, Del Prete D, Greco B, et al. (2012) Ryanodine Receptor Blockade Reduces Amyloid-beta Load and Memory Impairments in Tg2576 Mouse Model of Alzheimer Disease. J Neurosci. 32:11820-11834.

17. Iikuni S, Ono M, Watanabe H, et al. (2014) Enhancement of Binding Affinity for Amyloid Aggregates by Multivalent Interactions of ^{99m}Tc-Hydroxamamide Complexes. Mol Pharm 11:1132-1139.

18. Gonzalez J, Jurado-Coronel JC, Avila MF, Sabogal A, Capani F, Barreto GE (2015) NMDARs in neurological diseases: a potential therapeutic target. Int J Neurosci. 125:315-327.

19. Webster SJ, Bachstetter AD, Nelson PT, Schmitt FA, Van Eldik LJ (2014) Using mice to model Alzheimer's dementia: an overview of the clinical disease and the preclinical behavioral changes in 10 mouse models. Front Genet. 5:88.

20. Poisnel G, Herard AS, El Tayara NE, et al. (2012) Increased regional cerebral glucose uptake in an APP/PS1 model of Alzheimer's disease. Neurobiol Aging. 33:1995-2005.

21. Kuchibhotla KV, Lattarulo CR, Hyman BT, Bacskai BJ (2009) Synchronous Hyperactivity and Intercellular Calcium Waves in Astrocytes in Alzheimer Mice. Science 323:1211-1215.

22. Richards JG, Higgins GA, Ouagazzal AM, et al. (2003) PS2APP transgenic mice, coexpressing hPS2mut and hAPPswe, show age-related cognitive deficits associated with discrete

brain amyloid deposition and inflammation. *J Neurosci.* 23:8989-9003.

23. Schliebs R, Arendt T (2011) The cholinergic system in aging and neuronal degeneration.

Behav Brain Res 221:555-563.

24. Jin Y, Tsuchiya A, Kanno T, Nishizaki T (2015) Amyloid-beta peptide increases cell surface

localization of alpha 7 ACh receptor to protect neurons from amyloid beta-induced damage. *Biochem*

Biophys Res Commun. 468:157-160.

25. Wang H, Yu M, Ochani M, et al. (2003) Nicotinic acetylcholine receptor alpha 7 subunit is an

essential regulator of inflammation. *Nature* 421:384-388.

Figure 1

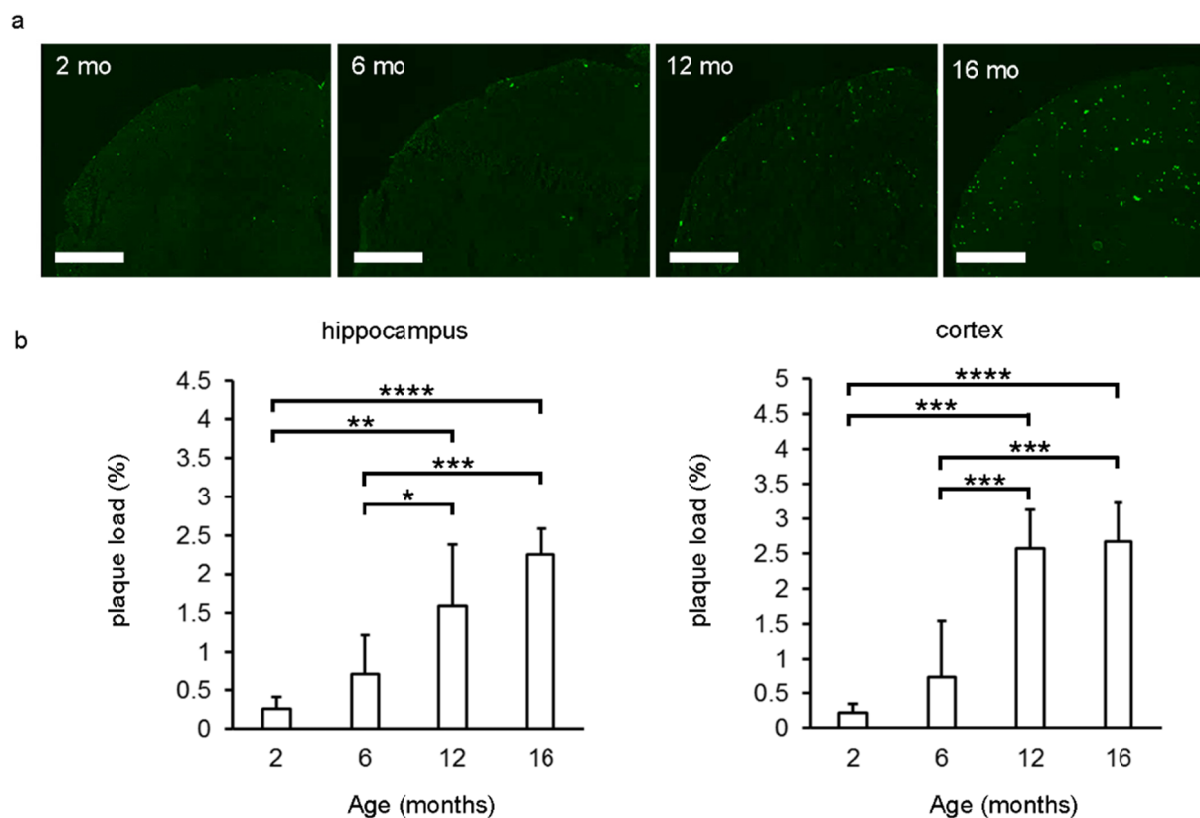


Fig. 1. Increased deposits of amyloid- β with aging in an APP/PS2 mouse brain.

Brain sections (10 μ m) at the level of the occipital cortex from APP/PS2 mice at 2, 6, 12, and 16 months of age were stained with thioflavin-S. (a) Representative fluorescence images and (b) summarized data of the A β accumulation at each age. Staining for amyloid deposits was detected at six months of age. After 12 months of age, the amyloid- β plaque loads in the hippocampus and cortex were significantly increased compared to 2 and 6 months of age (* P < 0.05, ** P < 0.01, *** P < 0.001, **** P < 0.0001 between indicated groups). Each column represents an average of 4 mice,

and each bar represents the SD.

Scale bars = 1000 μm . mo, month.

Figure 2

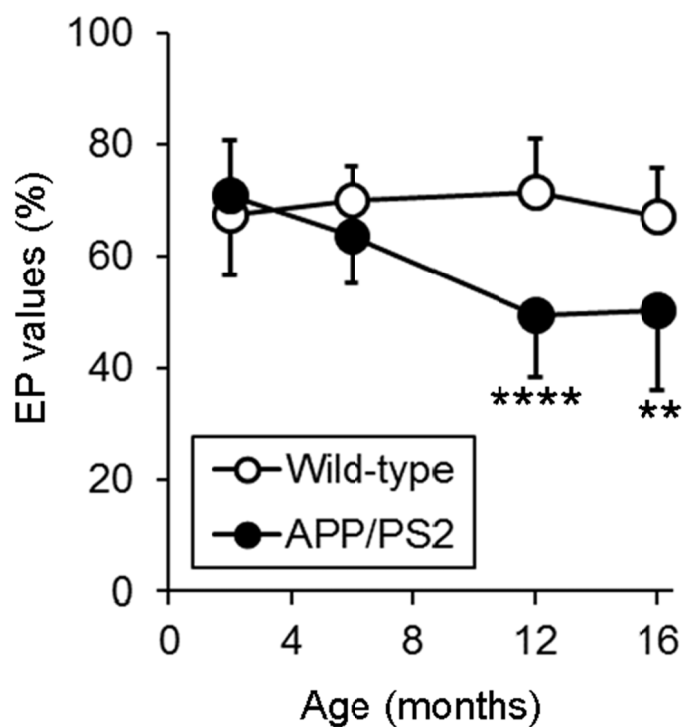


Fig. 2. Time-dependent changes in learning and memory abilities in APP/PS2 mice.

The NOR test was performed in APP/PS2 and wild-type mice at 2, 6, 12, and 16 months of age.

APP/PS2 mice showed a lower cognitive ability at 12 months of age (**** $P < 0.0001$ vs. wild-type mice) and at 16 months of age (** $P < 0.01$ vs. wild-type mice). Each point represents the average \pm

SD for 5–13 mice. EP, explore preference.

Figure 3

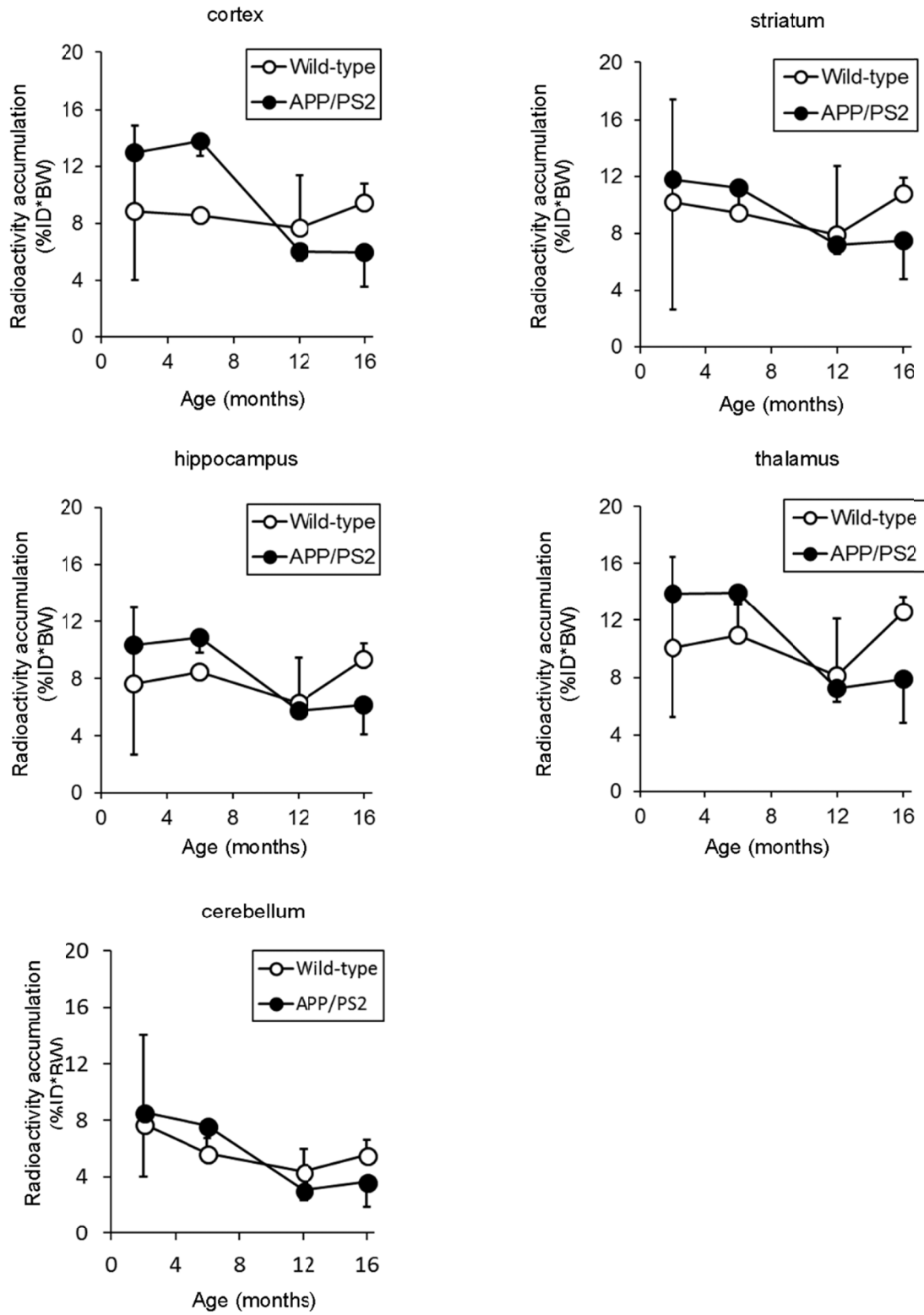


Fig. 3. Changes in [¹⁸F]FDG distribution in the brains of APP/PS2 mice.

The y-axes indicate the accumulation of [¹⁸F]FDG radioactivity in each brain region. No significant difference in glucose metabolism was observed in any brain region in APP/PS2 mice at 2, 6, 12, or 16 months of age as compared with in wild-type mice. Each point represents the average \pm SD for 4–5 mice.

Figure 4

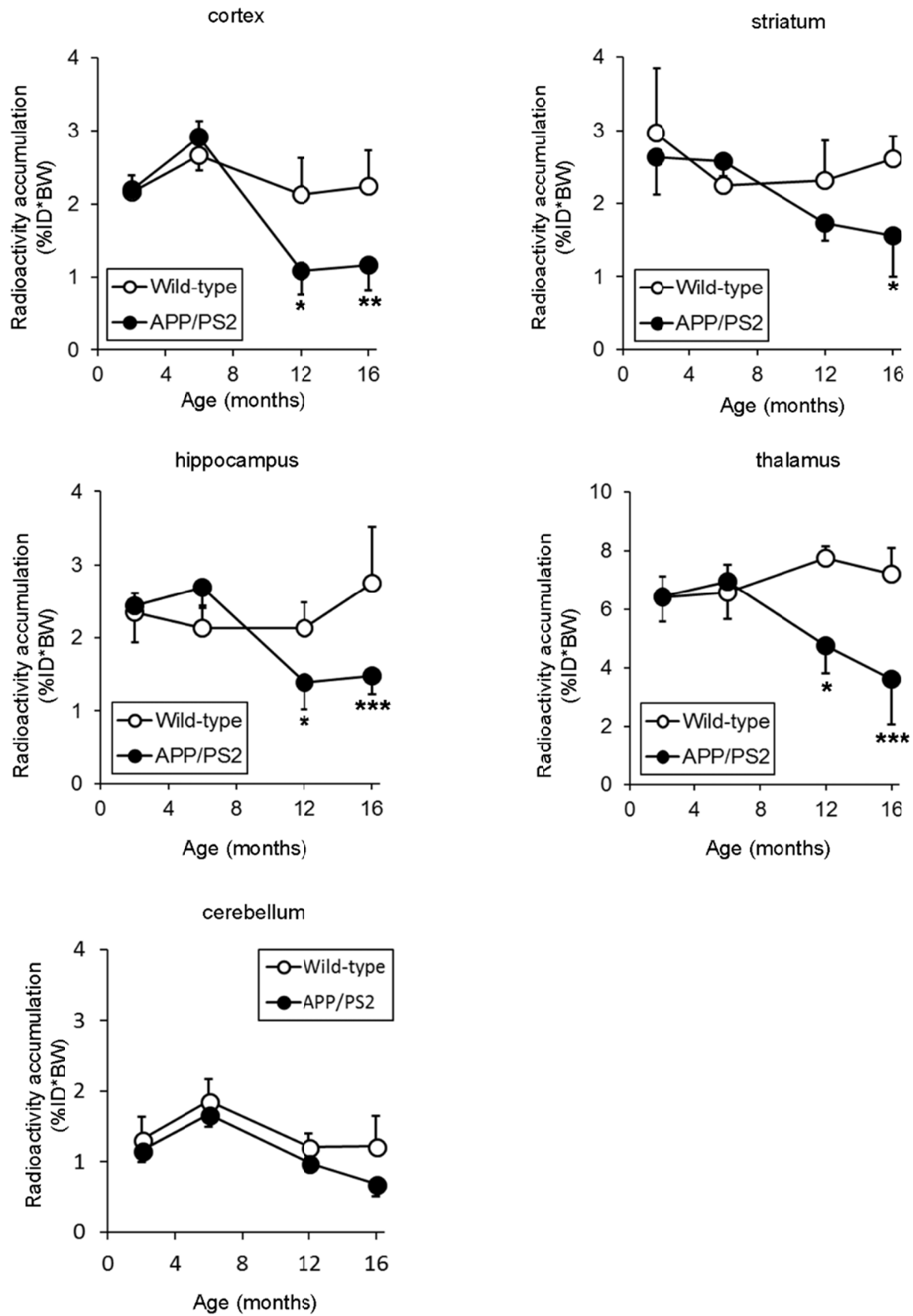


Fig. 4. Changes in [¹²⁵I]5IA distribution in the brains of APP/PS2 mice.

The y-axes indicate radioactivity accumulation of [¹²⁵I]5IA in each brain region. Notably, the APP/PS2 mice have a significant reduction in [¹²⁵I]5IA accumulation in the cortex, hippocampus, and thalamus at 12 months of age (**P* < 0.05 vs. wild-type) and in all brain regions at 16 months of age (**P* < 0.05 in the striatum, ***P* < 0.01 in the cortex, and ****P* < 0.0005 in the hippocampus and thalamus vs. wild-type). Each point represents the average ± SD for 4–5 mice.

Figure 5

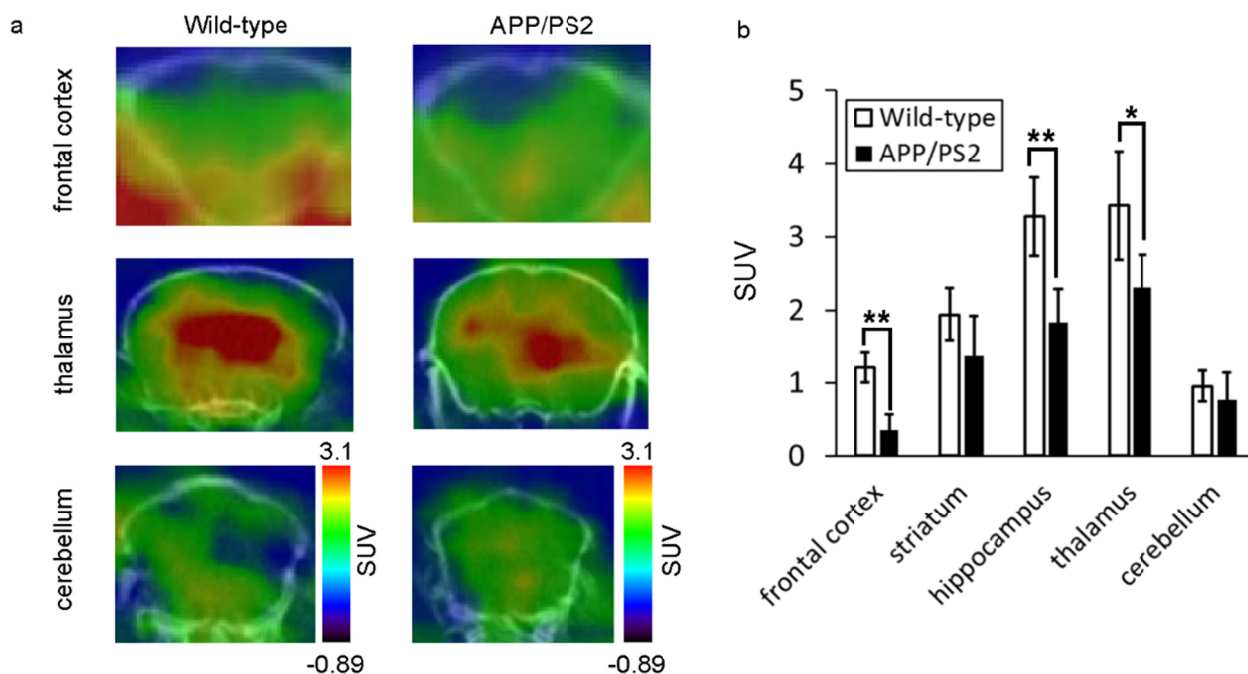


Fig. 5. *In vivo* [¹²³I]5IA-SPECT signal in the brains of APP/PS2 mice at 12 months of age

(a) Representative SPECT/CT images obtained 56 min after the injection of [¹²³I]5IA in the wild-type mice (*left*) and APP/PS2 mice (*right*) at 12 months of age. Images show slices at the frontal cortical, thalamic, and cerebellar levels, respectively. (b) The y-axes indicate SUVs in each brain region obtained 56 min after the injection of [¹²³I]5IA. A significant decrease is observed in the frontal cortex and hippocampus (** $P < 0.01$ vs. wild-type), and the thalamus (* $P < 0.05$ vs. wild-type). Each column represents an average of 4–5 mice, and each bar represents the SD. SUV, standardized uptake value.

Figure 6

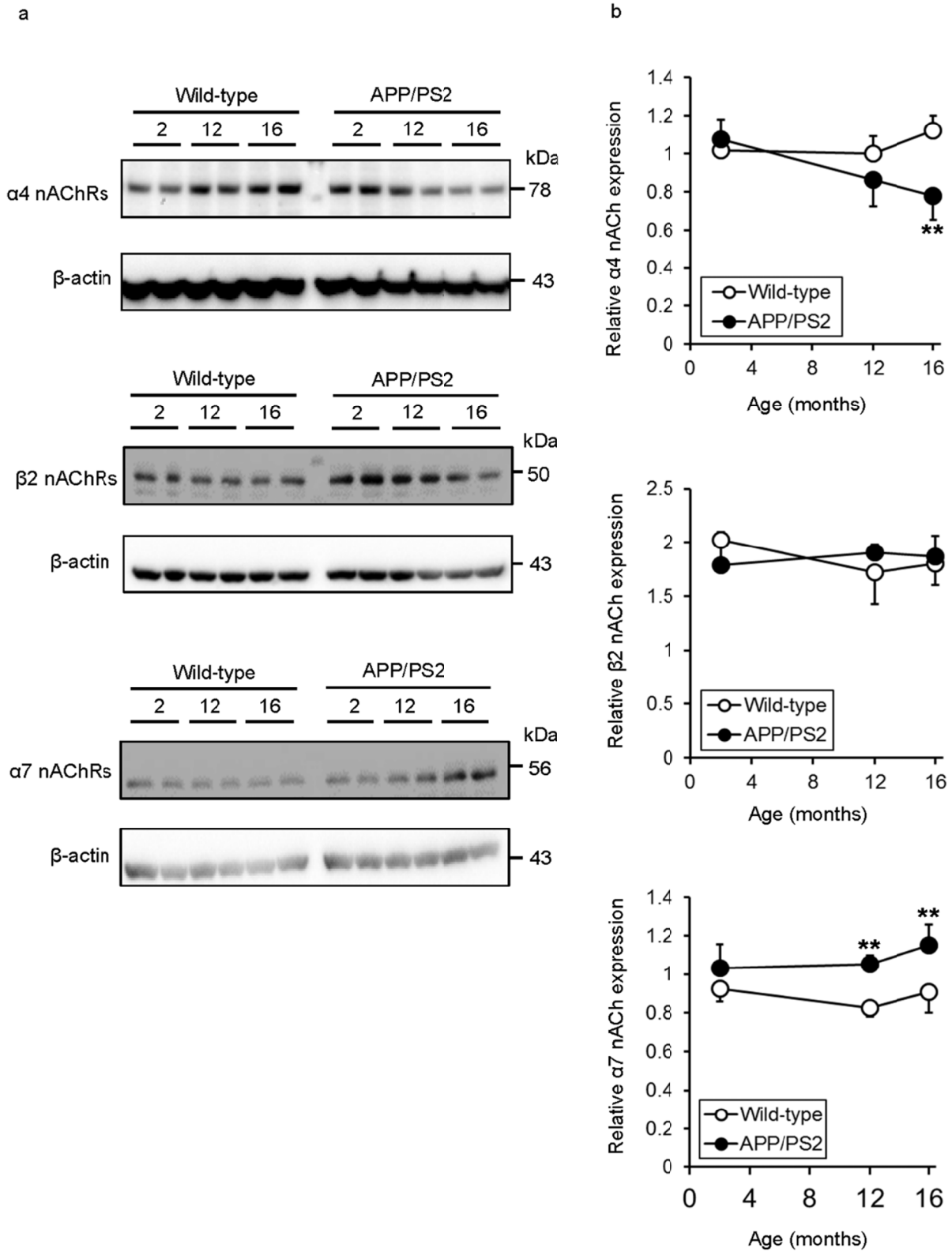


Fig. 6. nAChRs protein levels in the hippocampus of APP/PS2 mice.

The relative quantification of protein levels of $\alpha 4$, $\alpha 7$, and $\beta 2$ nAChRs in the hippocampus of APP/PS2 mice at 2–16 months of age was measured by Western blotting. (a) Representative immunoblots and (b) summarized data of Western blot analyses in the hippocampus of APP/PS2 mice. A significant decrease in $\alpha 4$ nAChRs levels was observed at 16 months of age (** $P < 0.01$ vs. wild-type) and a significant increase in $\alpha 7$ nAChRs was observed at 12 and 16 months of age (** $P < 0.01$ at 12 and 16 months of age vs. wild-type). Values are expressed relative to β -actin, and each point represents the average \pm SD for 4 mice.

Supplementary Material

Evaluation of the Relationship Between Cognitive Impairment, Glycometabolism, and Nicotinic Acetylcholine Receptor Deficits in a Mouse Model of Alzheimer's Disease

Yuki Matsuura¹, Masashi Ueda¹, Yusuke Higaki¹, Kohei Sano^{2,3}, Hideo Saji³, Shuichi Enomoto^{1,4}

¹Department of Biofunction Imaging Analysis, Graduate School of Medicine, Dentistry, and
Pharmaceutical Sciences, Okayama University, Japan

²Radioisotopes Research Laboratory, Kyoto University Hospital, Japan

³Department of Patho-Functional Bioanalysis, Graduate School of Pharmaceutical Sciences, Kyoto
University, Japan

⁴Next-Generation Imaging Team, RIKEN Center for Life Science Technologies, Japan

Supplementary Methods

RT-PCR analysis

APP/PS2 and wild-type mice at 2, 6, 12, and 16 months of age (n = 4 per group) were killed by cardiac puncture under anesthesia using 1.5–3% isoflurane. The brains were immediately removed and the hippocampus was isolated. RNA extraction, cDNA synthesis, and reverse transcription PCR (RT-PCR) were performed using the same procedure as that stated by Higashikawa *et al.* (1). The primer sequences, PCR product sizes, and accession number obtained from the Gene database are shown in Supplementary Table S2. The fluorescence intensities of the PCR products were quantitated using Image J software (NIH, MD, USA). The mRNA expression data was normalized to β -actin mRNA expression.

Animal tissue preparation and autoradiography analysis of [³H]MK-801

[³H]MK-801 were purchased from American Radiolabeled Chemicals Inc. (MO, USA). APP/PS2 and wild-type mice at 6, 12, and 16 months of age (n = 3–4 per group) were sacrificed by transcardial perfusion with phosphate buffered saline (PBS; pH 7.4) under anesthesia after completion of NOR analyses, and the brains were rapidly removed and frozen in a mixture of dry-ice and hexane (-75°C). Brain sections (10 μ m thickness) were cut on a microtome and mounted on glass slides. The slides were dried at 25°C overnight and then stored at -80°C.

Autoradiography analysis of the binding of [³H]MK-801 to NMDARs was performed using

a modification of the procedure by Velardo *et al.* (2). In brief, after preincubation, the sections were incubated for 120 min at 25°C in a buffer containing 10 nM [³H]MK-801 with 5 μM glycine and 5 μM L-glutamine, followed by washing for a total time of 1 h with 3 changes of ice cold buffer. The dried sections were exposed to imaging plates (BAS IP TR, Fuji Photo Film) for 20 h together with the calibrated ³H standards. The data were expressed in fmol/mg as the mean ± SD for all mice. Non-specific binding was measured in adjacent serial sections by incubation with 200 μM (+)MK-801 and was subtracted from the total binding in each brain region.

Supplementary Figure 1

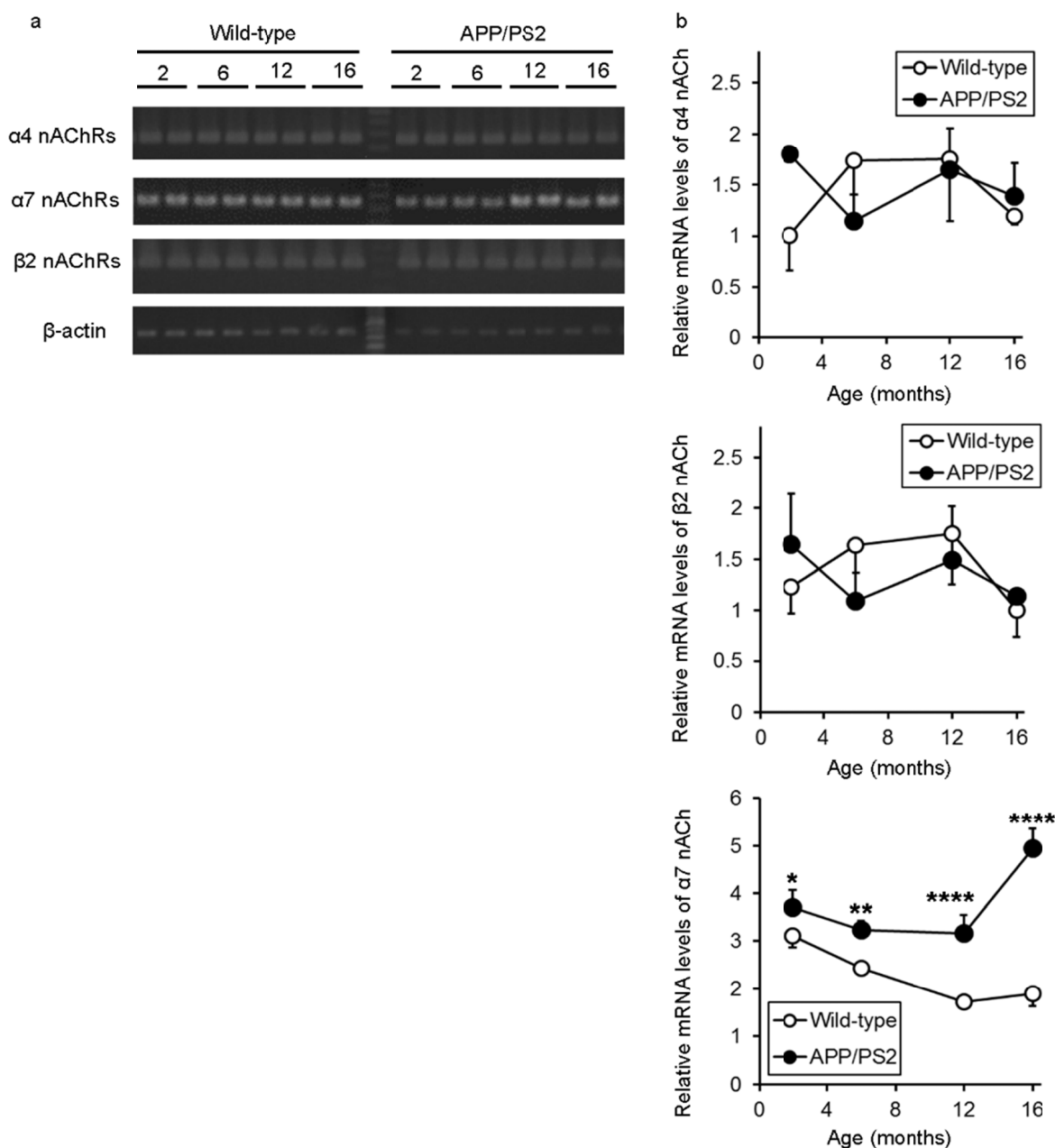


Fig. S1. Level of mRNA expression of nAChRs in the hippocampus of APP/PS2 mice

Relative quantification of mRNA levels of $\alpha 4$, $\alpha 7$, and $\beta 2$ nAChRs in the hippocampus of APP/PS2 mice at 2–16 months of age is measured by RT-PCR. (a) Representative gel images and (b) summarized data of RT-PCR analyses in the hippocampus of APP/PS2 mice. Significant increase in $\alpha 7$ nAChR levels is observed at 2, 6, 12, and 16 months of age (* $P < 0.05$ at 2 months of age, ** $P < 0.01$ at 6 months of age, **** $P < 0.0001$ at 12 and 16 months of age vs. wild-type). Values are expressed relative to β -actin and each point represents the average \pm SD for 4 mice.

Supplementary Figure 2

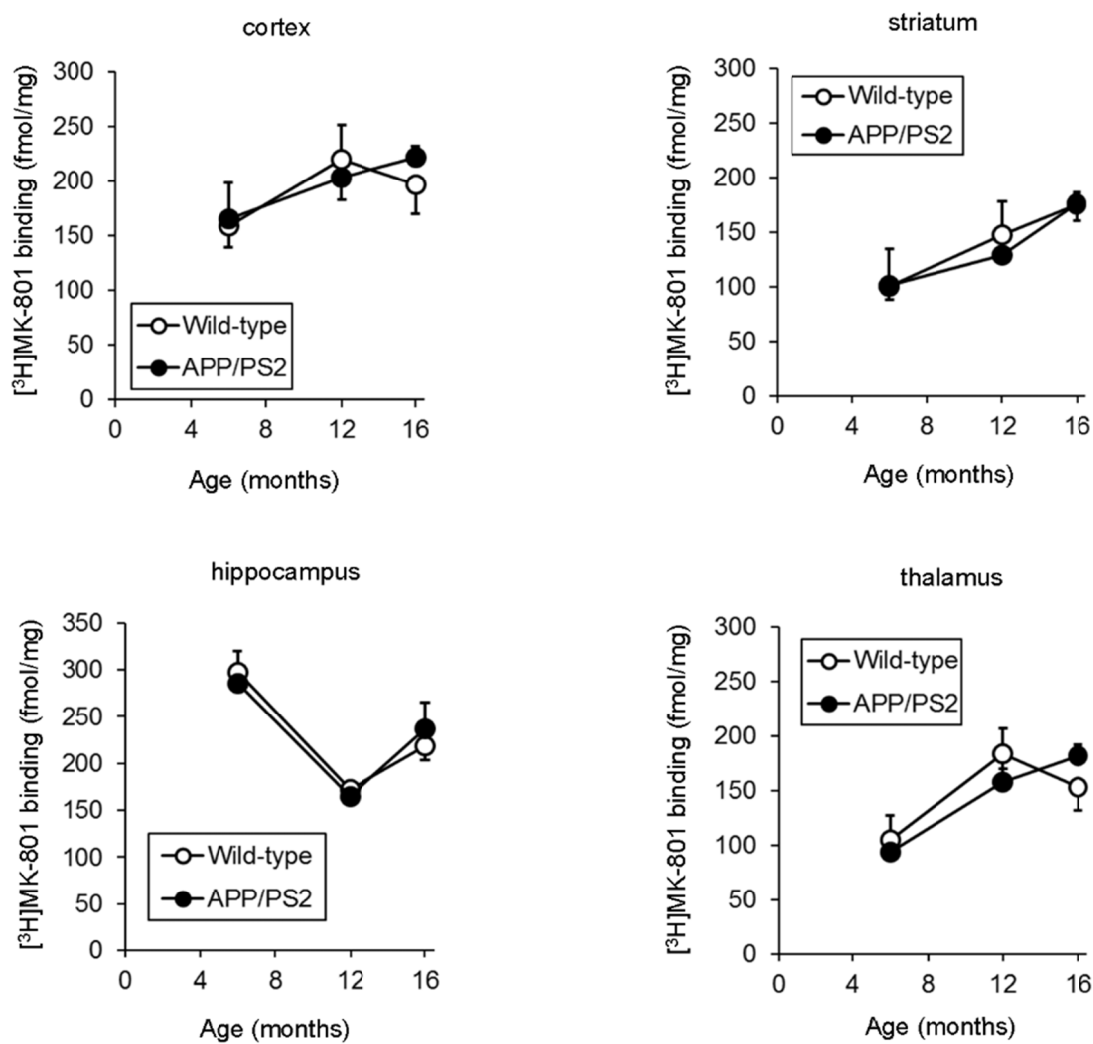


Fig. S2. Changes in $[^3\text{H}]$ MK-801 distribution in brains of APP/PS2 mice

No significant difference in $[^3\text{H}]$ MK-801 binding was observed in any brain region in APP/PS2 mice at 6, 12, or 16 months of age compared with wild-type mice. Each point represents an average of 3–4 mice, and each bar represents the SD.

Supplementary Tables

Table S1. Resources of antibodies and details for applications

Target	catalog #	antibody origin	Source	Dilution
$\alpha 4$	sc-5591	rabbit	Santa Cruz	1:750
$\beta 2$	sc-11372	rabbit	Santa Cruz	1:1000
$\alpha 7$	ab10096	rabbit	Abcam	1:500
β -actin	sc-47778	mouse	Santa Cruz	1:7500

The table shows the catalog number (#), antibody origin, source of antibody, and antibody dilution.

Table S2. Primers used for the amplification of mouse nAChRs and β -actin

Gene	oligo sequence (5' \rightarrow 3')	Product size (bp)	No
$\alpha 4$ nAChR	For CAGCTTCCAGTGTCAGACCA Rev ATGGCCACGTATTTCCAGTC	230	NM_015730.5
$\beta 2$ nAChR	For TGCTTTGTCAATCCTGCATC Rev TGGCAACGTATTTCCAATCC	199	NM_009602.4
$\alpha 7$ nAChR	For TCTGATTCCGTGCCCTTGATAG Rev CGCAGAAACCATGCACACC	173	NM_007390.3
β -actin	For CGGAACCGCTCATTGCC Rev ACCCACACT GTGCCATCTA	300	NM_007393

The table shows the nucleotide sequences, size of the amplified fragments in base pairs (bp), and the accession numbers (No) obtained from the Gene database.

Supplementary references

- (1) Higashikawa K, Yagi K, Watanabe K, et al. (2014) ^{64}Cu -DOTA-anti-CTLA-4 mAb enabled PET visualization of CTLA-4 on the T-cell infiltrating tumor tissues. PLoS ONE. 9:e109866.
- (2) Velardo MJ, Simpson VJ, Zahniser NR, et al. (1998) Differences in NMDA receptor antagonist-induced locomotor activity and ^3H -MK-801 binding sites in short-sleep and long-sleep mice. Alcohol clin Exp Res. 22: 1509-1515.